Nanoscale

PAPER

View Article Online
View Journal | View Issue

Cite this: *Nanoscale*, 2021, **13**, 10143

Metal-free bifunctional graphene oxide-based carbocatalysts toward reforming biomass from glucose to 5-hydroxymethylfurfural†

Minju Park, * Joonhee Lee and Byeong-Su Kim *

Received 31st March 2021,
Accepted 27th May 2021

DOI: 10.1039/d1nr02025k

rsc.li/nanoscale

Graphene oxide (GO) and its derivatives are promising metal-free heterogeneous catalysts due to their high surface area and rich chemical properties. We developed a bifunctional boron-doped sulfonated graphene oxide (BS-GO) and demonstrated its excellent catalytic conversion of glucose to 5-hydroxymethylfurfural (HMF) in a one-pot reaction. BS-GO afforded a high HMF yield of 36.0% from glucose without the use of additives or strong acids. Furthermore, the origin of the catalytic active sites of BS-GO was investigated, unveiling the unique bifunctional catalytic mechanism; it was revealed that two disjunct moieties, boronic acid and phenylsulfonic acid, in a single nanosheet of BS-GO catalyst have a bifunctional effect resulting in excellent catalytic production of HMF. This study suggests the potential of BS-GO as a green and sustainable carbocatalyst for reforming biomass to produce value-added chemicals. We anticipate that the unique structural design presented in this study will provide a guide to afford viable carbocatalysts for diverse organic reactions.

Introduction

The demand for energy is increasing rapidly worldwide, but the use of fossil fuels is not sufficient to satisfy this ever-increasing phenomenon. Moreover, the burning of fossil fuels is causing a large increase in greenhouse gases and decomposition of the carbon cycle.[1–3] The cumulative impact of fossil fuel utilization has prompted the search for alternative energy sources. In this context, biomass holds promise as a feedstock that is abundant, clean, and renewable for the production of biofuels and value-added chemicals.[4–8] Energy production from biomass has the advantage of forming less greenhouse gas compared with that from fossil fuels. Moreover, the carbon dioxide generated during energy production can be consumed during subsequent biomass regrowth.

Among the biomass feedstocks, the two most abundant carbohydrates, glucose and fructose, are ideal candidates to replace fossil fuels and hold significant potential as future energy resources.[9] To date, many approaches have been developed to provide efficient routes to convert biomass into valuable fuels and chemicals.[10–12] Among many of the bio-based products, furan-based compounds are rich sources of a variety of derivatives for fuel and chemical production. In particular, 5-hydroxymethylfurfural (HMF) is regarded as a key building block in the biomass conversion process. According to an evaluation by the U.S. Department of Energy, HMF is in the top ten bio-based chemicals due to its great potential for the production of fuel and bulk chemicals.[13–16] Although HMF can be easily obtained from fructose using a Brønsted acid at high temperature,[17,18] its conversion from glucose, the predominant monomer in cellulosic biomass, remains a significant challenge.[10]

When converting glucose to HMF, strong acid catalysts are typically required for each step, and thus significant research effort has been focused on the use of metal-based catalysts.[9,18–20] However, they are toxic despite their good catalytic activity, which raises concerns about their sustainability and environmental issues. Alternatively, homogeneous Brønsted and Lewis acid catalysts such as H_2SO_4, HCl, and boric acid (H_3BO_3) have been introduced, albeit with moderate glucose conversion performances (Table S1†).[21–23] In previous research by Ståhlberg and coworkers, boric acid was used as a cocatalyst to produce HMF from glucose.[23] The diol structure of boric acid forms a stable complex with the carbohydrates and promotes the isomerization of glucose. Although boric acid produces a good HMF yield without the use of a metal complex, homogeneous catalysts often suffer from poor product separation, recycling, and problems with corrosion. In this context, discovering rational strategies toward environmentally benign and effective catalysts remains an important issue.

Department of Chemistry, Yonsei University, Seoul 03722, Republic of Korea.
E-mail: minju143@yonsei.ac.kr, bskim19@yonsei.ac.kr

†Electronic supplementary information (ESI) available: Detailed characterizations, XPS, Raman spectra, HPLC analysis, and additional figures and tables (PDF). See DOI: 10.1039/d1nr02025k

With this in mind, graphene oxide (GO) and its derivatives are promising metal-free heterogeneous catalysts due to their unique physical and chemical properties, including atomically thin two-dimensional structures with a high surface area, easy recyclability, and a variety of functional groups.[24–28] For example, GO contains epoxides and hydroxyl groups on the basal planes whereas carboxylic acids and other functional groups are present at the edge sites, which can be further tailored to various functionalities.[29–33] In this context, GO and its derivatives can serve as an ideal platform for catalytic conversion.[28] Thus far, several groups have successfully demonstrated the use of GO and its derivatives as carbocatalysts for synthetic transformations such as oxidation,[24] C–H activation,[34] epoxide ring-opening,[35] acid or base reactions,[36] oxidative coupling,[37,38] and Friedel–Crafts alkylation.[39]

Although there has been preceding research on the use of metal-free catalysts including metal–organic framework and mesoporous organosilica materials to convert fructose to HMF,[40–42] few cases have used glucose or cellulose as the starting substrate due to the challenges in the processing.[43] Recently, Chen *et al.*[44] utilized sulfonated graphene quantum dots as a non-metallic catalyst to convert glucose to HMF. However, it has low catalytic activity for glucose conversion and its quasi-heterogeneous structure limits its facile recycling. Furthermore, Pan *et al.* reported the synthesis of bifunctional porous polymers bearing boronic and sulfonic acids, which demonstrated good catalytic activity as a new type of cellulase-mimetic solid acids to hydrolyze cellulose to glucose.[45]

We report herein a unique strategy to produce HMF directly from glucose catalyzed by novel bifunctional metal-free carbocatalysts based on GO nanosheets (Scheme 1), as a part of our on-going interest in the development of graphene-based catalysts. Specifically, we introduced two distinct types of catalytic moieties, boronic acid and phenylsulfonic acid, onto GO nanosheets to afford boron-doped sulfonated graphene oxide (BS-GO). The tailored GO-based catalyst with unique bifunctional groups demonstrated significantly improved catalytic performance for HMF production compared to homogeneous catalysts. Furthermore, the GO-derivatives were easily recyclable using a simple centrifugation method, which highlights the advantage of using heterogeneous catalysts. Finally, we propose a putative mechanism for the conversion of glucose to HMF based on ^{1}H NMR analysis, which suggests a unique bifunctional catalytic effect involving the boronic acid and phenylsulfonic acid groups in BS-GO. We believe that our method provides a versatile strategy for the customization of GO-based catalysts to achieve high performance in a desirable synthetic reaction through the appropriate choice of functional moieties.

Results and discussion

Synthesis of the GO-derivatives

In the initial stage of our investigation, chemically modified GO-based carbocatalysts were synthesized from exfoliated GO nanosheets (Fig. 1a). In brief, a GO suspension was synthesized following a modified Hummers' method.[46,47] As it is expected that boron atoms provide immobilized active sites during the catalytic reaction of glucose isomerization, they were introduced onto the GO nanosheets *via* thermal annealing of GO in the presence of boric acid. This resulted in the incorporation of boron into the graphene framework in different configurations with respect to oxygen ($-BC_xO_y$: $-BC_2O$ or $-BCO_2$) and carbon ($-BC_3$) in the graphene lattice (B-GO, hereafter).[48,49] Subsequently, the resulting B-GO was chemically functionalized by the direct anchoring of sulfonic acid-containing aryl radicals. In this step, the phenylsulfonic acid moiety was grafted onto the basal plane of graphene *via* diazo-

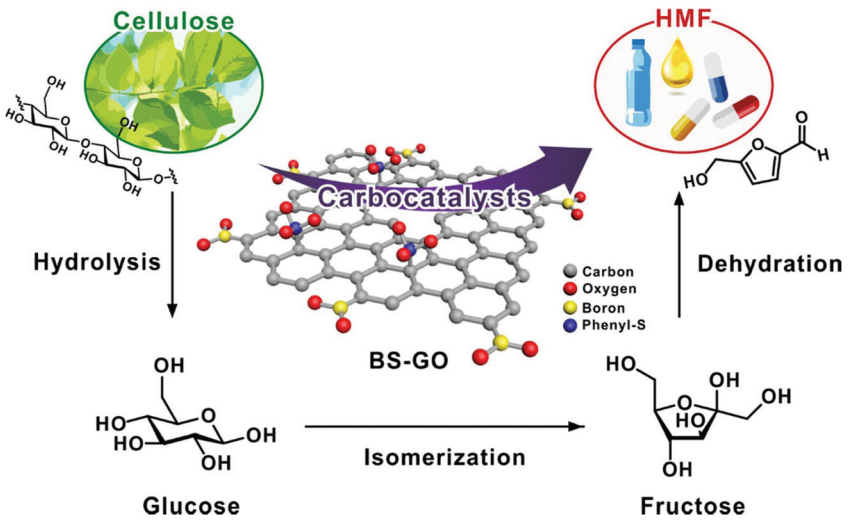

Scheme 1 Schematic representation of the catalytic conversion of biomass to HMF. BS-GO, boron-doped sulfonated graphene oxide; phenyl-S, the phenylsulfonic acid group; HMF, 5-hydroxymethylfurfural.

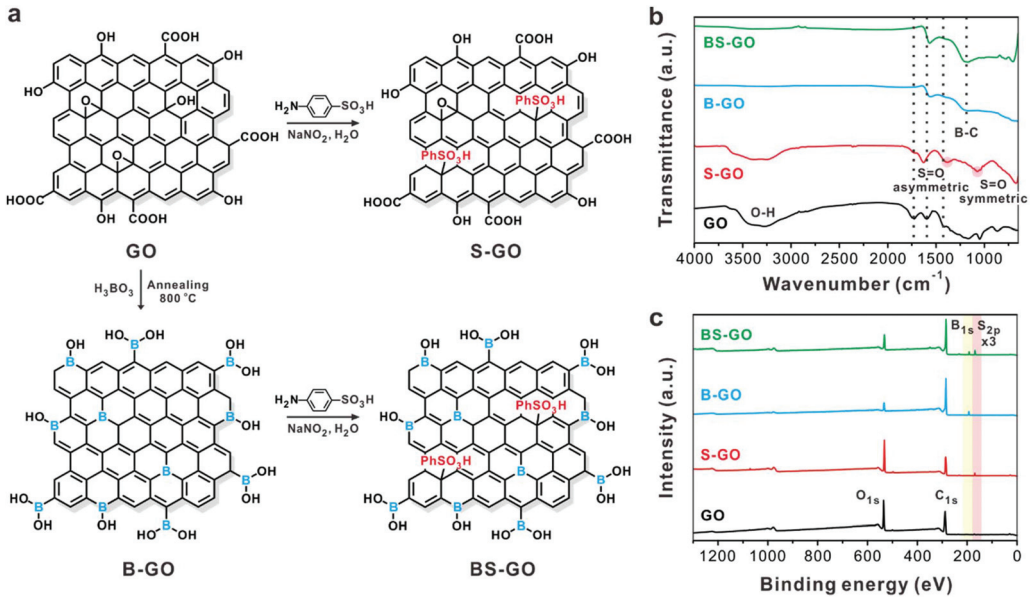

Fig. 1 (a) Synthetic approaches to the GO-based carbocatalysts, (b) FT-IR spectra, and (c) XPS survey spectra of the GO-based carbocatalysts used in this study. GO, graphene oxide; B-GO, boron-doped graphene oxide; BS-GO, boron-doped sulfonated graphene oxide; S-GO, sulfonated graphene oxide.

nium chemistry.[50,51] Owing to its low pK_a value (−6.62), the phenylsulfonic acid group can provide a Brønsted acidic site in catalytic reactions.[52] Finally, BS-GO was prepared as a bifunctional carbocatalyst as described above. As the control, S-GO was prepared to clarify the roles of the active sites in the carbocatalysts.

Successful chemical modification of GO was confirmed *via* FT-IR analysis. The FT-IR spectra revealed that the pristine GO presented three characteristic peaks at 3200–3500, 1725, and 1315 cm^{-1}, attributable to hydroxyl (–OH), carboxylic acid (–COOH), and epoxy (C–O–C) groups, respectively (Fig. 1b).[53] Moreover, a characteristic peak at 1594 cm^{-1} indicated the presence of C=C bonds within the sp^2-network of graphene. Compared to that of GO, the C=C vibration peak for S-GO was slightly blue-shifted from 1594 to 1625 cm^{-1}, which indicates the partial conversion of the sp^2-graphitic lattice upon sulfonation.[54] Additional peaks appeared at 1382 and 1072 cm^{-1}, which were assigned as asymmetric and symmetric S=O stretching, thus confirming the presence of the sulfonic acid group.[50,51] After introducing boron into the GO to produce B-GO, the overall intensity of the oxygen functional groups was significantly reduced due to their removal upon annealing. The C=C vibration peaks in both B-GO and BS-GO were red-shifted from 1594 to 1558 cm^{-1}, thereby indicating the reduction of GO.[54] The boron doping was confirmed by the appearance of new peaks corresponding to B–C (1153 cm^{-1}) and B–O (~1000 cm^{-1}) in both B-GO and BS-GO.[49,53]

The presence of boron species and phenylsulfonic acid groups was further investigated through XPS analysis (Fig. 1c). Pristine GO showed the presence of only carbon and oxygen atoms, with a trace amount of sulfur originating from the sulfuric acid in the GO synthesis.[52] It was also found that significant boron content (approximately 4.78 at%) incorporated into B-GO during the annealing process that was absent in the pristine GO and S-GO (Table S2†). Similarly, the C/O ratio of B-GO increased from 2.59 to 9.73, indicating that oxygen functional groups were removed by the annealing process. Moreover, the amount of boron in BS-GO was almost unchanged (4.15 at%) during functionalization with the sulfonic acid group. The slight decrease in the C/O ratio from B-GO to BS-GO implies that sulfonic acid groups were successfully grafted onto the graphene sheets. The deconvoluted high-resolution B 1s XPS spectrum elucidated the different types of boron configurations bonded to oxygen (–BC_xO_y (–BC_2O or –BCO_2): 190.98 eV) and carbon (–BC_3: 192.68 eV) on the graphene nanosheets (Fig. S1†).[49] The content of –BC_xO_y in BS-GO was slightly decreased from 66.6 to 40.0 at% compared to B-GO since some of the boronic acid sites were detached upon introduction of the phenylsulfonic acid groups.

Meanwhile, structural changes during functionalization were investigated *via* Raman spectroscopic analysis (Fig. S2). GO presented two prominent bands, the symmetric A_{1g} mode of the D band (1346 cm^{-1}) and the E_{2g} mode of the G band (1597 cm^{-1}).[55] The D band is related to disordered carbon lattices in, for instance, defects, edges, or amorphous structures, while the G band corresponds to in-phase vibration of the graphitic sp^2-carbon lattice. The I_D/I_G intensity ratio for S-GO was slightly higher due to the introduction of phenylsulfonic acid groups onto the sp^2-carbon lattice. Similarly, the I_D/I_G ratios of B-GO and BS-GO were higher than that of pristine GO due to the boron doping.

The dispersion stability of the GO-derivatives is another useful tool to determine chemical functionalization (Fig. S3†). While B-GO lost its aqueous dispersibility due to the removal

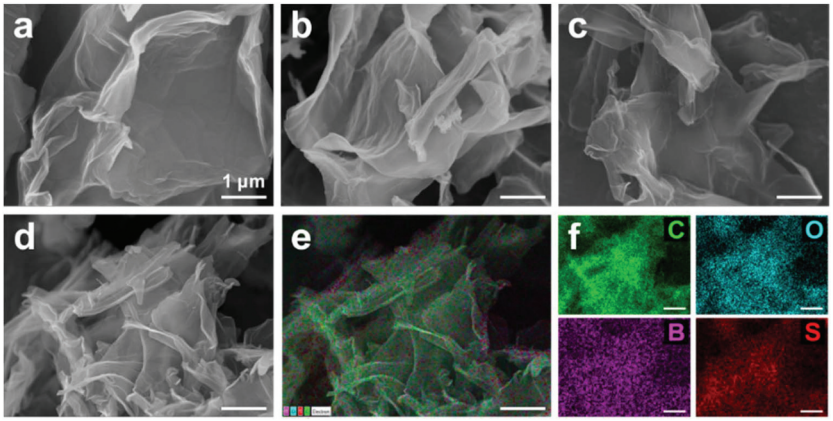

Fig. 2 SEM images of (a) GO, (b) S-GO, (c) B-GO, and (d) BS-GO. (e and f) Corresponding EDS elemental mapping images of BS-GO for each designated atom. The scale bars indicate 1 μm.

of oxygen-containing functional groups in the annealing process, BS-GO presented good dispersion behavior as the charged sulfonate groups prevented the graphene sheets from aggregation. The structures and morphologies of the carbocatalysts were analyzed using SEM; all of the GO-based carbocatalysts clearly possessed crumpled and wrinkled paper-like morphologies (Fig. 2). This reflects that the synthetic approach, *i.e.* boron-doping and the diazonium reaction, did not alter the intrinsic morphology of the graphene nanosheet. Moreover, the EDS imaging of the BS-GO nanosheets indicates that boron and sulfur were uniformly distributed in BS-GO nanosheets. Taken together, these results indicate that boronic acid and phenylsulfonic acid groups were successfully introduced into the graphene lattice.

Catalytic reaction to convert glucose to HMF

The synthesized GO-derivatives were tested as metal-free catalysts for producing HMF from biomass. It is well known that HMF can be selectively produced from fructose or other sugars in DMSO, as the DMSO itself acts as a catalyst[56–58] by promoting the formation of the furanoid form of fructose and facilitating its subsequent dehydration to HMF. As a preliminary experiment, we confirmed that the HMF yield from fructose in DMSO was high even in the absence of a catalyst (Tables S3 and S4†). Moreover, all of the carbocatalysts exhibited much improved catalytic activity of approximately 80%, even with a short reaction time of 1 h (entries 3–10 in Table S4†). Interestingly, GO demonstrated an excellent conversion performance of 88% within 1 h, which originated from the Brønsted acidic sites of the carboxylic acid groups in the GO nanosheet. In the same context, S-GO presented the best catalytic activity due to the presence of the Brønsted acidic sites both phenylsulfonic acid and the carboxylic acid groups. The decrease in HMF yield over B-GO and BS-GO could originate from their structures. As shown by the XPS measurement, oxygen-containing functional groups were detached during the annealing process, resulting in a decrease in Brønsted acid density (Table S2†). Moreover, the diol structure of boronic acid can form a stable diboron intermediate complex with fructose, which can inhibit its dehydration to HMF (Scheme S1†).[23]

Based on these results, we explored the reactivity of glucose with GO-derivatives in DMSO (Table S5†). Unfortunately, they showed a very low HMF yield of less than 8% even at high temperatures and long reaction times. Therefore, the solvent was changed to the sugar-solubilizing ionic liquid, 1-ethyl-3-methylimidazolium chloride ([EMIM]Cl), which has been reported to be an efficient medium for reforming biomass to HMF.[9,59] First, the reaction temperature and time were optimized with the BS-GO catalyst in [EMIM]Cl (Fig. S4 and Table S6†). Under conditions of 130 °C for 3 h, the maximum HMF yield was achieved, which equates to an improvement of up to 21.0%.

Table 1 lists the results for HMF yield from the conversion of glucose under different reaction conditions. In general, catalytic activity was improved with an increase in the reaction temperature from 100 to 130 °C (entries 2–4 in Table 1). However, the yield decreased marginally over 130 °C due to the formation of undesired byproducts such as rehydration compounds and condensation products (Table 1, entry 5). Since byproducts were considerably condensed, which resulted in insoluble humins or polymeric structures, it was limited to identify by using HPLC and NMR analyses. In addition, we investigated the influence of catalyst concentration on catalytic performance (entries 4, 6, 9 in Table 1). Unexpectedly, the yield gradually decreased from 36.0% to 21.0% with the increase in catalyst load. A similar observation was reported for the use of a boric acid promoter for the dehydration of glucose.[23] Specifically, at high concentrations of boric acid catalyst, a stable diboron-fructose complex formed, which was responsible for inhibiting the conversion of fructose (Scheme S1†). Since it is difficult to decompose the diboron-fructose complex into fructose, the subsequent dehydration of fructose to HMF was inhibited. This phenomenon clearly explains why the B-GO and BS-GO catalysts produced lower HMF yields from fructose than the GO catalyst (entries 7–10 in

Table 1 HMF yields from glucose by the GO-based carbocatalysts prepared in this study

Entry	Catalyst	Mass (mg)	Temperature (°C)	Time (h)	HMF Yield (%)
1	No catalyst	0	130	3	15.2
2	BS-GO	10	100	3	7.8
3	BS-GO	10	120	3	18.2
4	BS-GO	10	130	3	21.0
5	BS-GO	10	140	3	12.2
6	BS-GO	5.0	130	3	23.1
7	BS-GO	2.5	130	1	34.4
8	BS-GO	2.5	130	2	35.7
9	BS-GO	2.5	130	3	36.0
10	GO	2.5	130	3	13.2
11	S-GO	2.5	130	3	15.2
12	B-GO	2.5	130	3	31.4
13	Phenylboronic acid	2.5	130	3	33.6

Reaction conditions: 0.1 g of glucose, 1.0 mL of [EMIM]Cl, under an air atmosphere. HMF, 5-hydroxymethylfurfural; GO, graphene oxide; B-GO, boron-doped graphene oxide; BS-GO, boron-doped sulfonated graphene oxide; S-GO, sulfonated graphene oxide.

Table S4†). More extensive screening was performed by varying the reaction time for the production of HMF from glucose *via* the BS-GO catalyst (entries 7–9 in Table 1). The conversion of glucose was almost completed within 1 h, with the yield of HMF only slightly increasing over a longer reaction time. The maximum yield of up to 36.0% was achieved within 3 h, which is a 2.4-fold improvement over the non-catalyzed reaction.

Fig. 3 and Table S7† present a summary of the catalytic conversion of glucose to HMF with the carbocatalysts. Although pristine GO did not enhance the conversion of glucose to HMF (entry 10 in Table 1), both S-GO and B-GO showed improved performances (entries 11 and 12 in Table 1), with BS-GO producing the best HMF yield of 36.0%. After boron was introduced into GO (B-GO), the conversion of glucose was rapidly increased from 38.2 to 87.4%. Furthermore, the yield of HMF was highly improved from 13.2 to 31.4%, which implies that the boronic acid site plays a vital role in this catalytic system. To confirm the contribution of the boronic acid sites in this catalytic transformation, phenylboronic acid was used as a molecular analog of the carbocatalytic system to mimic its catalytic activity (entry 13 in Table 1). Impressively, it exhibited a 33.6% yield of HMF, which is comparable to that of BS-GO. All these results strongly indicate that introducing boronic acid into GO-derivatives plays a critical role in converting glucose to HMF. Boronic acid incorporated can provide active catalytic sites to isomerize glucose to fructose, which is the main rate-determining step for the overall reaction. In addition, phenylsulfonic group can provide a Brønsted acidic site in catalytic reactions to additionally improve the HNF yield by accelerating hydration of fructose. As such, the BS-GO catalyst containing both boronic and Brønsted acid sites was more effective in producing HMF than the catalysts incorporating the individual boronic (B-GO) and Brønsted (S-GO) acid sites. The two disjunct moieties, boronic acid and phenylsulfonic acid, demonstrate a unique bifunctional effect in a single nanosheet of BS-GO catalyst, resulting in excellent catalytic performance.

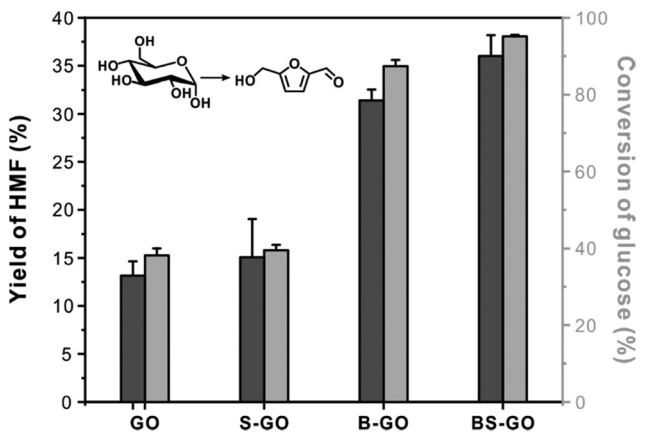

Fig. 3 HMF yields and conversion of glucose over the carbocatalysts. Reaction conditions: glucose 0.5 g, solvent 5.0 mL, catalysts 12.5 mg, 130 °C, and under an air atmosphere. GO, graphene oxide; B-GO, boron-doped graphene oxide; BS-GO, boron-doped sulfonated graphene oxide; S-GO, sulfonated graphene oxide. The average values with standard deviation were collected from three independent experiments.

The glucose to HMF conversion mechanism

To date, the non-stoichiometric nature of GO has presented a considerable challenge toward understanding the catalytic mechanism of carbocatalysts.[60] Several groups have reported unique methods of investigating the mechanisms of a variety of reactions involving GO-based carbocatalysts. As a notable example, Loh's group tried to overcome this limitation by using electron spin resonance (ESR) spectroscopy to examine the origin of the catalytic active sites of GO.[61] In the present study, we introduced glucose deuterated at the C-2 position (D-glucose-2-d_1) to identify the carbocatalytic mechanism of HMF production from glucose (Fig. 4a). The reaction of deuterated glucose can produce different ratios of isotope-labeled products according to the reaction pathway.

In general, there are two possible pathways from glucose to HMF: the hydride transfer route and the ene-diol route. The detailed mechanistic pathway is represented in Fig. S5.† In short, during the hydride transfer route, deuterium is transferred to afford fructose exclusively deuterated at the C-1 position. Accordingly, subsequent dehydration reaction from fructose to HMF would theoretically result in 50% of deuterated HMF result in the final product. In contrast, in the ene-diol mechanism as suggested in this study, a ketone forms at the C-2 position of glucose that eliminates all the deuterium. Thus, no deuterium is incorporated in the HMF molecule as the final product. It is well known that Cr-based catalysts and the glucose isomerase enzyme follow the hydride transfer route (Fig. 4a). We compared the reaction mechanisms of the BS-GO and $CrCl_2$ catalysts by using deuterated glucose. In the ^1H NMR spectra presented in Fig. 4b, the integration ratio between the C-1 and C-4 positions of HMF was approximately

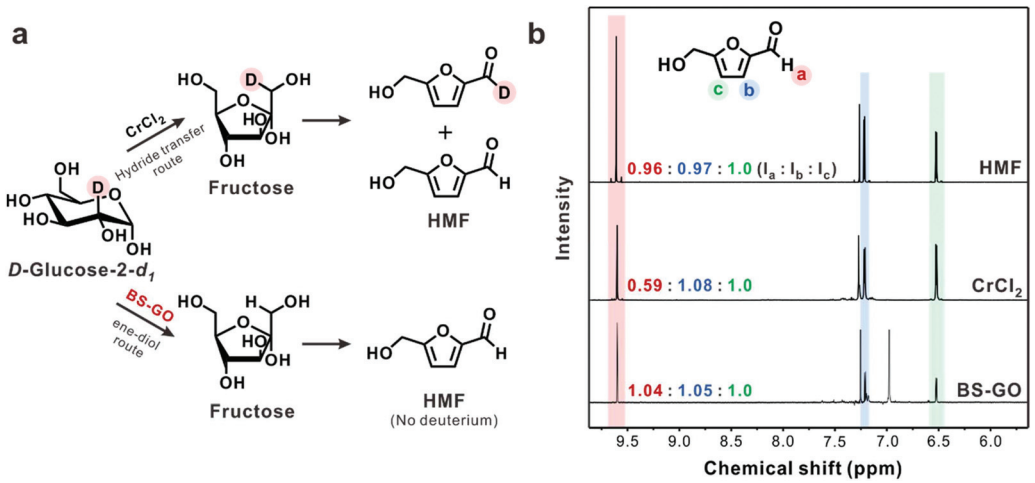

Fig. 4 (a) Two representative reaction pathways from D-glucose-2-d_1 to HMF and (b) ^{1}H NMR spectra of standard HMF and HMF produced from deuterated glucose, using $CrCl_2$ and boron-doped sulfonated graphene oxide (BS-GO) catalysts. Reaction conditions: glucose 0.1 g, solvent 1.0 mL, catalyst 2.5 mg, 130 °C, and under an air atmosphere. All spectra were collected in $CDCl_3$.

0.59 (I_a/I_c) when the Cr-based catalyst was used, which implies that 41% of the HMF molecules were deuterated. The BS-GO catalyzed reaction proceeded *via* a different reaction mechanism compared to the Cr-based catalyst. All of the deuterium was eliminated and the ratio of C-1 to C-4 was approximately 1.04 (I_a/I_c), clearly displaying that the isomerization of glucose to fructose over BS-GO proceeds *via* an ene-diol intermediate, which is unlike the mechanism over metal-based catalysts.

Based on these results, we propose a putative mechanism for the conversion of glucose to HMF over the BS-GO catalyst (Scheme 2). The selective isomerization of glucose can proceed through the formation of an ene-diol intermediate. First, a boronic acid site forms a complex with a glucose diol (compound **a**). An open-chain glucose-boronic acid, coordinated to the 3- and 4-positions is then generated (compound **b**). The chelating effect of the boronic acid stabilizes the open-chain complex and the O–B–O angle becomes less strained in open-chain glucose. Subsequently, the acidic conditions cause O1 to become protonate, resulting in an ene-diol intermediate (compound **c**). Proton exchange then forms a closed-ring structure (compound **d**). Finally, BS-GO is regenerated upon the formation of fructose. Subsequently, the Brønsted acidic phenylsulfonic acid groups (-SO_3H) serve as catalytic active sites for the dehydration of fructose to HMF.

Recyclability testing. Recycling for up to five cycles was conducted to verify the utility of BS-GO as a heterogeneous catalyst. Fig. 5 shows the isolated yields of HMF *via* the catalytic regeneration experiment. As noted, the bifunctional BS-GO carbocatalyst presents good recyclability and can be reused after simple centrifugation and rinsing with methanol and water. Although there was a slight decrease in activity up to the 5th cycle (from 34.7% to 28.1%), the catalytic performance remains comparable to that of homogeneous catalysts. To verify the reduced catalytic activity, post-BS-GO was collected after the 5th cycle and investigated *via* XPS (Table S8†). Even after 5 cycles, the boron content was almost unchanged (approximately 4.93 at%). Since boron was introduced onto the GO nanosheets *via* thermal annealing process, boron contain-

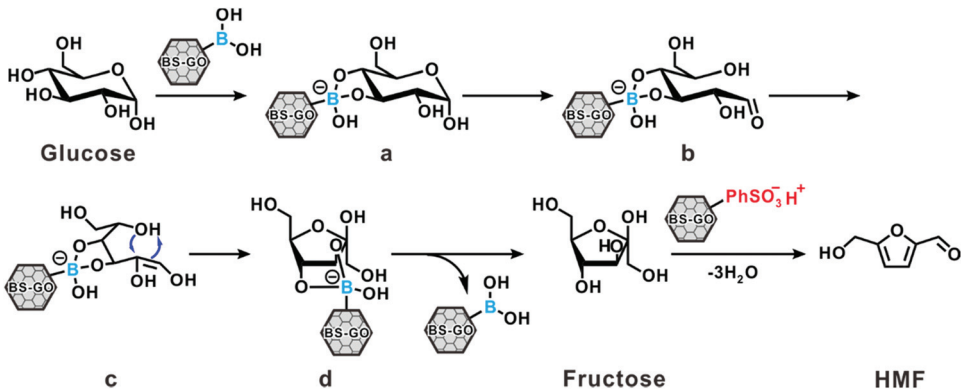

Scheme 2 The putative mechanism for HMF production from glucose with BS-GO as the catalyst.

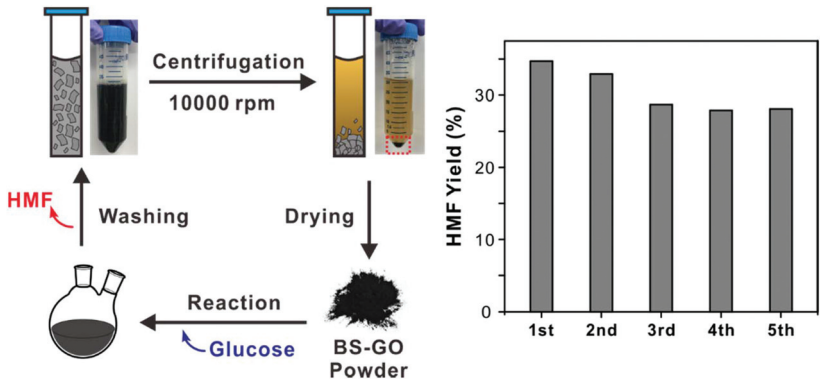

Fig. 5 Recyclability testing of the BS-GO catalyst for the production of HMF from glucose. Reaction conditions: glucose 1.0 g, solvent 10 mL, catalyst 25 mg, 130 °C, 3 h, and under an air atmosphere.

ing functional groups were stable even at high temperatures during catalytic reaction. On the other hand, the sulfur content was reduced from 1.67 to 0.13 at%, resulting in slightly decreased catalytic performance after each cycle. Nevertheless, high yields were achieved with low catalyst loading of BS-GO, which is unprecedented in carbocatalyst research and demonstrates its high potential for practical applications.

Conclusion

We developed metal-free bifunctional GO-based carbocatalysts and demonstrated that BS-GO is highly efficient and robust in the direct conversion of glucose into HMF in a one-pot reaction. Two disjunct moieties, boronic acid and phenylsulfonic acid, show a unique bifunctional effect in a single nanosheet of BS-GO catalyst, resulting in excellent catalytic performance for the production of HMF from glucose. Owing to the heterogeneous structure of BS-GO, it was easily reusable and the HMF yield was satisfactory up to 5 cycles. Furthermore, we investigated the catalytic mechanism using analog molecules and deuterated glucose to determine the origin of the active sites. In the BS-GO catalyst, the boronic acid sites play a critical role in converting glucose to HMF. Selective isomerization of glucose proceeded through the formation of an ene-diol intermediate, and the Brønsted acidic phenylsulfonic acid, completed the reaction by dehydrating fructose to HMF. Although the catalytic performance is lower than that of metal-based and homogeneous catalysts, we anticipate that graphene-derivatives will be viable catalysts in diverse organic reactions and offer advantages in terms of sustainability as green catalysts.

Experimental details

Preparation of the carbocatalysts

Initially, graphite oxide powder was prepared using a modification of Hummers' method, and a brown dispersion of graphene oxide (GO) was prepared by exfoliation *via* sonication, resulting in a concentration of 1.0 mg mL^{-1}. To synthesize boron-doped graphene oxide (B-GO), dried GO powder (0.1 g) was mixed uniformly with boric acid (0.1 g) and thermally annealed at 800 °C for 2 h under an argon atmosphere.[49] Subsequently, phenylsulfonic acid groups were introduced *via* diazonium chemistry to produce BS-GO.[51] B-GO was dispersed under sonication (conc. 1.0 mg mL^{-1}). The aryl diazonium salt was prepared in water from the reaction of sulfanilic acid (460 mg) and sodium nitrite (200 mg) in 100 mL of water. After 1.0 M HCl solution (7.0 mL) was added to this mixture in an ice bath, the solution color changed from pale yellow to colorless. The dispersion was stored in the ice bath for more than 2 h and then subjected to extensive dialysis (Spectra/Por MWCO 12–14 K, Thermo Fisher Scientific, USA) for 4 d to remove any byproducts and remaining reactants. For the control experiment, GO was phenylsulfonated using the same method as used for BS-GO but without the boron-doping process, resulting in sulfonated GO (S-GO).

Structural characterization

FT-IR spectroscopy in ATR-mode (wavenumber range: 650–4000 cm^{-1}; Varian 670, Agilent Scientific Instruments, USA) was used to identify the chemical structures of the GO-derivatives. X-ray photoelectron spectroscopy (XPS; K-alpha, Thermo Fisher Scientific) was used to determine the elemental compositions and the chemical bonding of the GO-derivatives. The heteroatom-doping and structural changes were confirmed by Raman spectroscopy (LabRam Aramis, Horiba Scientific, USA). The structures and morphologies of the carbocatalysts were analyzed using scanning electron microscopy (SEM) with energy-dispersive X-ray spectroscopy (EDS) mapping (JEOL-7800F, JEOL Ltd, Japan).

Catalytic performance for producing HMF

1-Ethyl-3-methylimidazolium chloride ([EMIM]Cl) (1.0 g) was melted at 80 °C, after which glucose (100 mg) and a catalyst (2.5 mg) were added. Glucose deuterated at the C-2 position (D-glucose-2-d_1), and chromium dichloride ($CrCl_2$) were added

to identify the catalytic mechanism. The concentration of reaction intermediates was measured *via* high-performance liquid chromatography (HPLC, Prominence HPLC system, Shimadzu Scientific Instruments, USA) equipped with a Shim-pack GIS C18 (5 μm; 250 mm length × 4.6 mm diameter) column, refractive index (RI) detector, and an ultraviolet (UV) detector (265 nm) using 9 : 1 (v/v) water: methanol as the mobile phase. The flow rate was constant at 1.0 mL min^{-1} and the injection volume was 5 μm. For the recycling process, the mixture was washed with water and methanol and centrifuged at 10 000 rpm for 20 min.

Author contributions

M.P. and B.-S.K. conceptualized the article, designed the experiments, supervised the projects, and wrote the draft of the manuscript. J.L. analyzed the NMR measurement.

Conflicts of interest

There are no conflicts to declare.

Acknowledgements

This work was supported by the National Research Foundation of Korea (NRF-2017M3A7B4052802 and NRF-2018R1A5A1025208). This research was supported by the Yonsei University Research Fund of 2018.

References

1 R. Bailis, M. Ezzati and D. M. Kammen, *Science*, 2005, **308**, 98–103.
2 J. Goldemberg, *Science*, 2007, **315**, 808–810.
3 B. R. Caes, M. J. Palte and R. T. Raines, *Chem. Sci.*, 2013, **4**, 196–199.
4 G. W. Huber, J. N. Chheda, C. J. Barrett and J. A. Dumesic, *Science*, 2005, **308**, 1446–1450.
5 E. M. Rubin, *Nature*, 2008, **454**, 841–845.
6 Y. J. Zhou, E. J. Kerkhoven and J. Nielsen, *Nat. Energy*, 2018, **3**, 925–935.
7 H. Wang, Y. Pu, A. Ragauskas and B. Yang, *Bioresour. Technol.*, 2019, **271**, 449–461.
8 B. Kumar, N. Bhardwaj, K. Agrawal, V. Chaturvedi and P. Verma, *Fuel Process. Technol.*, 2020, **199**, 106244.
9 H. Zhao, J. E. Holladay, H. Brown and Z. C. Zhang, *Science*, 2007, **316**, 1597–1600.
10 M. Besson, P. Gallezot and C. Pinel, *Chem. Rev.*, 2014, **114**, 1827–1870.
11 M. G. Davidson, S. Elgie, S. Parsons and T. J. Young, *Green Chem.*, 2021, **23**, 3154–3171.
12 H. Zhang, S. Wang, H. Zhang, J. H. Clark and F. Cao, *Green Chem.*, 2021, **23**, 1370–1381.
13 R.-J. van Putten, J. C. van der Waal, E. de Jong, C. B. Rasrendra, H. J. Heeres and J. G. de Vries, *Chem. Rev.*, 2013, **113**, 1499–1597.
14 J. J. Bozell and G. R. Petersen, *Green Chem.*, 2010, **12**, 539–554.
15 T. Werpy and G. Petersen, *Top Value Added Chemicals from Biomass Volume I—Results of Screening for Potential Candidates from Sugars and Synthesis Gas*, U. S. D. Energy, 2004.
16 L. Zhu, X. Fu, Y. Hu and C. Hu, *ChemSusChem*, 2020, **13**, 4812–4832.
17 D. W. Brown, A. J. Floyd, R. G. Kinsman, Y. Roshanhyphen and Y. Ali, *J. Chem. Technol. Biotechnol.*, 1982, **32**, 920–924.
18 J. B. Binder and R. T. Raines, *J. Am. Chem. Soc.*, 2009, **131**, 1979–1985.
19 E. A. Pidko, V. Degirmenci, R. A. van Santen and E. J. M. Hensen, *Angew. Chem., Int. Ed.*, 2010, **49**, 2530–2534.
20 Y. Wei, Y. Zhang, B. Li, C. Yan, Z. Da, M. Meng, C. Liu and Y. Yan, *Energy Technol.*, 2020, **8**, 1901111.
21 L. Qi, Y. F. Mui, S. W. Lo, M. Y. Lui, G. R. Akien and I. T. Horváth, *ACS Catal.*, 2014, **4**, 1470–1477.
22 M. Chidambaram and A. T. Bell, *Green Chem.*, 2010, **12**, 1253–1262.
23 T. Ståhlberg, S. Rodriguez-Rodriguez, P. Fristrup and A. Riisager, *Chem. – Eur. J.*, 2011, **17**, 1456–1464.
24 D. R. Dreyer, H.-P. Jia and C. W. Bielawski, *Angew. Chem., Int. Ed.*, 2010, **49**, 6813–6816.
25 C. Su and K. P. Loh, *Acc. Chem. Res.*, 2013, **46**, 2275–2285.
26 D. R. Dreyer and C. W. Bielawski, *Chem. Sci.*, 2011, **2**, 1233–1240.
27 S. Navalon, A. Dhakshinamoorthy, M. Alvaro and H. Garcia, *Chem. Rev.*, 2014, **114**, 6179–6212.
28 E. K. Jeon, E. Seo, E. Lee, W. Lee, M.-K. Um and B.-S. Kim, *Chem. Commun.*, 2013, **49**, 3392–3394.
29 S. Stankovich, D. A. Dikin, R. D. Piner, K. A. Kohlhaas, A. Kleinhammes, Y. Jia, Y. Wu, S. T. Nguyen and R. S. Ruoff, *Carbon*, 2007, **45**, 1558–1565.
30 T. Lee, E. K. Jeon and B.-S. Kim, *J. Mater. Chem. A*, 2014, **2**, 6167–6173.
31 M. Karthik and P. Suresh, *ACS Sustainable Chem. Eng.*, 2019, **7**, 9028–9034.
32 M.-T. Li, M. Liu, Y.-H. Yu, A.-W. Li and H.-B. Sun, *Bull. Chem. Soc. Jpn.*, 2019, **92**, 283–289.
33 K. Ariga, E. Ahn, M. Park and B.-S. Kim, *Chem. – Asian J.*, 2019, **14**, 2553–2566.
34 Y. Gao, P. Tang, H. Zhou, W. Zhang, H. Yang, N. Yan, G. Hu, D. Mei, J. Wang and D. Ma, *Angew. Chem., Int. Ed.*, 2016, **55**, 3124–3128.
35 H. R. Thomas, A. J. Marsden, M. Walker, N. R. Wilson and J. P. Rourke, *Angew. Chem., Int. Ed.*, 2014, **53**, 7613–7618.
36 F. Zhang, H. Jiang, X. Li, X. Wu and H. Li, *ACS Catal.*, 2014, **4**, 394–401.
37 M. Shaikh, A. Sahu, A. K. Kumar, M. Sahu, S. K. Singh and K. V. S. Ranganath, *Green Chem.*, 2017, **19**, 4533–4537.
38 C. Su, R. Tandiana, J. Balapanuru, W. Tang, K. Pareek, C. T. Nai, T. Hayashi and K. P. Loh, *J. Am. Chem. Soc.*, 2015, **137**, 685–690.

39 F. Hu, M. Patel, F. Luo, C. Flach, R. Mendelsohn, E. Garfunkel, H. He and M. Szostak, *J. Am. Chem. Soc.*, 2015, **137**, 14473–14480.
40 H. Wang, Q. Kong, Y. Wang, T. Deng, C. Chen, X. Hou and Y. Zhu, *ChemCatChem*, 2014, **6**, 728–732.
41 M. Shaikh, S. K. Singh, S. Khilari, M. Sahu and K. V. S. Ranganath, *Catal. Commun.*, 2018, **106**, 64–67.
42 Q. Hou, W. Li, M. Ju, L. Liu, Y. Chen and Q. Yang, *RSC Adv.*, 2016, **6**, 104016–104024.
43 P. Bhanja, A. Modak, S. Chatterjee and A. Bhaumik, *ACS Sustainable Chem. Eng.*, 2017, **5**, 2763–2773.
44 K. Li, J. Chen, Y. Yan, Y. Min, H. Li, F. Xi, J. Liu and P. Chen, *Carbon*, 2018, **136**, 224–233.
45 Q. Yang and X. Pan, *ACS Sustainable Chem. Eng.*, 2016, **4**, 4824–4830.
46 W. S. Hummers and R. E. Offeman, *J. Am. Chem. Soc.*, 1958, **80**, 1339–1339.
47 M. Park, T. Lee and B.-S. Kim, *Nanoscale*, 2013, **5**, 12255–12260.
48 Y. Zheng, Y. Jiao, L. Ge, M. Jaroniec and S. Z. Qiao, *Angew. Chem., Int. Ed.*, 2013, **52**, 3110–3116.
49 Z.-H. Sheng, H.-L. Gao, W.-J. Bao, F.-B. Wang and X.-H. Xia, *J. Mater. Chem.*, 2012, **22**, 390–395.
50 Y. Si and E. T. Samulski, *Nano Lett.*, 2008, **8**, 1679–1682.
51 J. Ji, G. Zhang, H. Chen, S. Wang, G. Zhang, F. Zhang and X. Fan, *Chem. Sci.*, 2011, **2**, 484–487.
52 M. Park, K. Song, T. Lee, J. Cha, I. Lyo and B.-S. Kim, *ACS Appl. Mater. Interfaces*, 2016, **8**, 21595–21602.
53 M. Acik, G. Lee, C. Mattevi, M. Chhowalla, K. Cho and Y. J. Chabal, *Nat. Mater.*, 2010, **9**, 840–845.
54 X. Xu, T. Yuan, Y. Zhou, Y. Li, J. Lu, X. Tian, D. Wang and J. Wang, *Int. J. Hydrog. Energy*, 2014, **39**, 16043–16052.
55 K. N. Kudin, B. Ozbas, H. C. Schniepp, R. K. Prud'homme, I. A. Aksay and R. Car, *Nano Lett.*, 2008, **8**, 36–41.
56 R. Liu, J. Chen, X. Huang, L. Chen, L. Ma and X. Li, *Green Chem.*, 2013, **15**, 2895–2903.
57 F. W. Lichtenthaler and S. Rönninger, *J. Chem. Soc., Perkin Trans. 2*, 1990, 1489–1497, DOI: 10.1039/P29900001489.
58 Y. Román-Leshkov, J. N. Chheda and J. A. Dumesic, *Science*, 2006, **312**, 1933–1937.
59 H. Ohno, M. Yoshizawa-Fujita and Y. Kohno, *Bull. Chem. Soc. Jpn.*, 2019, **92**, 852–868.
60 X. Fan, G. Zhang and F. Zhang, *Chem. Soc. Rev.*, 2015, **44**, 3023–3035.
61 C. Su, M. Acik, K. Takai, J. Lu, S.-j. Hao, Y. Zheng, P. Wu, Q. Bao, T. Enoki, Y. J. Chabal and K. P. Loh, *Nat. Commun.*, 2012, **3**, 1298.